Recent progress in MXene-based nanomaterials for high-performance aqueous zinc-ion hybrid capacitors

ZHANG Ming-hui[1,†], XU Wen[1,†], WU Li-sha[1], DONG Yan-feng[1,2,*]

(1. *Department of Chemistry*, *College of Sciences*, *Northeastern University*, *Shenyang* 110819, *China*;
2. *CAS Key Laboratory of Carbon Materials*, *Institute of Coal Chemistry*, *Chinese Academy of Sciences*, *Taiyuan* 030001, *China*)

Abstract: Aqueous zinc-ion hybrid capacitors (ZHCs) have an intrinsic safety and low cost, and are promising for use in large-scale energy storage devices. However, traditional porous carbon cathodes have inappropriate pore structures for zinc ion storage and diffusion. Moreover, zinc foil anodes suffer from the growth of Zn dendrites and side reactions, so that traditional ZHCs usually have a non-competitive energy density and unsatisfactory service life, seriously inhibiting their practical use. Two-dimensional transition metal carbide/nitride MXenes with a highly conductive matrix and abundant surface functional groups are good choices for constructing high-capacity cathodes and long-life Zn anodes for high-performance ZHCs. Recent progress in MXene-based nanomaterials as electrode materials of advanced ZHCs is summarized. The fundamentals of ZHCs are first introduced, such as working principles and key electrochemical parameters. The use of various MXene-based cathodes and anodes in high-performance aqueous ZHCs are then considered and, finally, the challenges and prospects for MXene-based nanomaterials for next-generation ZHCs are briefly discussed.

Key words: Zinc-ion hybrid capacitors; MXene; Cathodes; Anodes

1 Introduction

Batteries usually provide high energy density and operating voltage, nevertheless their power density and cycle life are not satisfied[1, 2]. While, supercapacitors have advantages in power output, rate capability and cycle life, unfortunately, low energy density is a bottle-neck for their practical applications[3]. Hybrid capacitors not only have the advantages of high energy density of batteries, but also possess the long life of supercapacitors, which are promising in large-scale energy storage applications (e.g., electric vehicles)[4–6]. The past decade has witnessed the fast development of various organic electrolyte based hybrid capacitors, such as lithium-ion hybrid capacitors[7, 8], sodium-ion hybrid capacitors[9], potassium-ion hybrid capacitors[10], however, the safety concerns of organic electrolyte based hybrid capacitors may seriously impede their commercial applications. In this regard, the emerging aqueous zinc-ion hybrid capacitors (ZHCs) have attracted more attention owing to their advantages of long cycle life, high energy density and high power density[11]. Moreover, metal zinc possesses low cost ($65 kWh^{-1} vs. $300 kW h^{-1} of metal Li), high theoretical capacity of 820 mAh g^{-1} and low redox potential of −0.76 V (vs. standard hydrogen electrode), which guarantees outstanding compatibility in mild aqueous electrolytes with high ionic conductivity and effectively avoids the safety concerns of organic electrolytes[11–15]. Generally, ZHCs are usually composed of capacitive electrodes, battery electrodes, electrolytes, and separators. The capacitive electrode materials mainly refer to carbon materials or pseudocapacitive materials[16–18]. The battery electrode materials mainly include metal zinc, or vanadium/manganese-based oxides. However, the low capacity of traditional carbon cathodes and dendrite problems are the fatal challenges of present ZHCs, which leads to unsatisfied electrochemical performance, such as low energy density and short service life[11, 19].

As a type of emerging two-dimensional (2D) materials after graphene, MXenes have the chemical formula of $M_{n+1}X_nT_x$ (n=1-3), where M, X, and T refer to early transition metals (e.g., Ti, V, Cr, Zr, Nb) and carbon and/or nitrogen, and the surface terminations (e.g., —O, —OH, —F, —Cl)[20], respectively.

Received date: 2022-03-02; **Revised date:** 2022-04-19

Corresponding author: DONG Yan-feng, Associate Professor. E-mail: dongyanfeng@mail.neu.edu.cn

Author introduction: †ZHANG Ming-hui and XU Wen contributed equally to this work.

MXenes are usually synthesized by selectively etching away a atomic layer in the MAX phase, where A represents elements in groups 13-16 of the periodic table (e.g., Al, Si, Sn)[21]. Ti_3C_2 MXene was for the first time synthesized by etching Ti_3AlC_2 with HF acid in 2011 (Fig. 1a). MXenes possess atomically thin nanosheets, high conductivity (6 000-8 000 S cm^{-1})[22, 23], high Young's modulus up to 0.33±0.03 TPa for $Ti_3C_2T_x$ [24], and fast ion diffusion coefficient (e.g., 10^{-10} to 10^{-9} cm^2 s^{-1} for Li^+ in $Ti_3C_2T_x$)[25], and good dispersibility in a variety of solvents[26]. Consequently, MXenes have been frequently employed as electrode materials in various energy storage devices[27–31]. MXenes possess good hydrophilicity and conductivity simultaneously, showing promising applications in aqueous ZHCs. However, the first work on MXene for ZHCs was not reported until 2019. Since then, MXenes were widely employed in both cathodes and anodes of ZHCs (Fig. 1b-i)[32–39]. For example, Sn^{4+} was inserted into MXene to enlarge its interlayer spacing, which effectively avoided the restacking of MXene to achieve an ultralong lifespan of up to 2 800 h (Fig. 1c)[33]. N-doped MXene-based heterostructure could prevent MXene from easy oxidization at high potentials, and even in a wide voltage range from 0.2 to 1.8 V, the capacity retention rate remained 87.1% after 9 000 cycles (Fig. 1d)[34]. Yang et al.[36] prepared nanoscale Zn anodes by vertically depositing Zn nanosheets on Ti_3C_2 films, which were degradable in waste devices during recycling (Fig. 1f). Although several literatures have focused on the carbon cathodes, anodes and electrolytes in ZHCs[3, 40, 41], the application of MXene-based nanomaterials for both cathodes and anodes in advanced ZHCs in terms of material preparation and structural design has not been reported yet.

Herein, we systematically review the latest advance of MXene-based nanomaterials for cathodes and anodes in the state-of-the-art ZHCs. Specially, MXene based cathodes are divided into pure MXenes, intercalated MXenes, doped MXenes, and MXene based hybrids, and MXene based Zn anodes are elaborated as MXene coatings on Zn and MXene based hosts for Zn (Fig. 2). Finally, the challenges and pro-

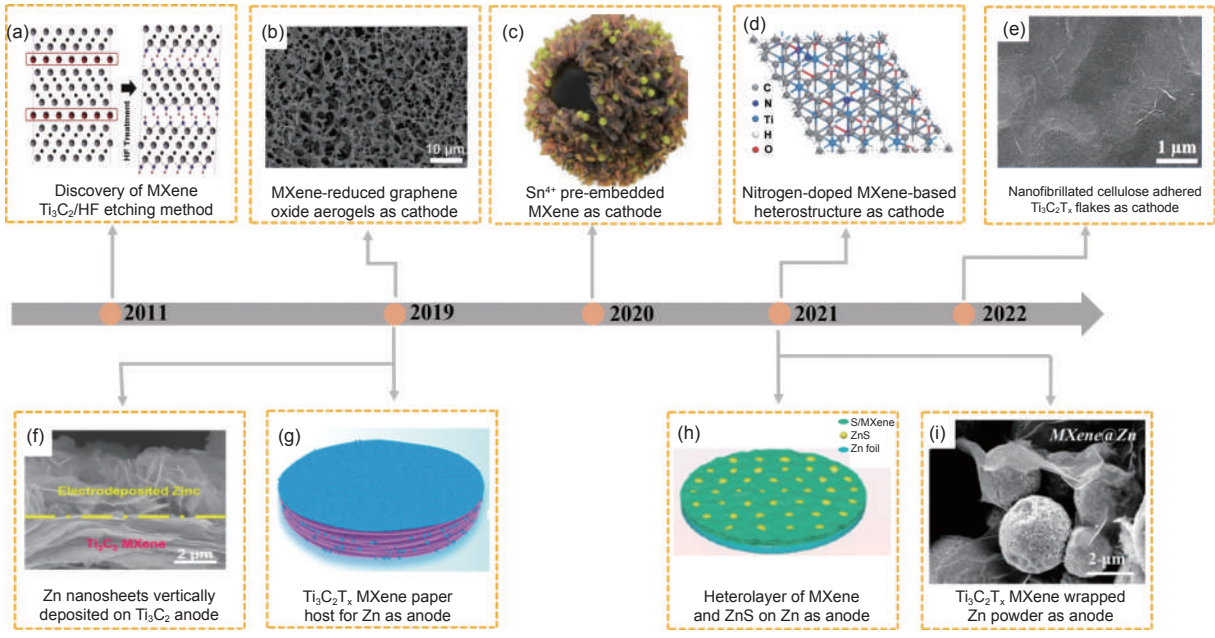

Fig. 1　Main progress of MXene-based nanomaterials for ZHCs. (a) MXene was firstly obtained by selective etching of Al in Ti_3AlC_2 with HF acid[42] (Reprinted with permission by copyright 2011, Wiley). (b) MXene-reduced graphene oxide aerogels as the cathode[32](Reprinted with permission by copyright 2019, Wiley). (c) Sn^{4+} pre-embedded MXene cathode[33] (Reprinted with permission by copyright 2020, Wiley). (d) Nitrogen-doped MXene-based heterostructure cathode[34] (Reprinted with permission by copyright 2021, RSC). (e) Nanofibrillated cellulose adhered $Ti_3C_2T_x$ flake cathode[35](Reprinted with permission by copyright 2022, Elsevier). (f) Zn nanosheets vertically deposited on Ti_3C_2 MXene [36] (Reprinted with permission by copyright 2019, ACS). (g) $Ti_3C_2T_x$ MXene paper host for Zn [37] (Reprinted with permission by copyright 2021, ACS). (h) Heterolayer of MXene and ZnS on Zn[38] (Reprinted with permission by copyright 2021, ACS). (i) $Ti_3C_2T_x$ MXene wrapped Zn powder[39] (Reprinted with permission by copyright 2021, ACS).

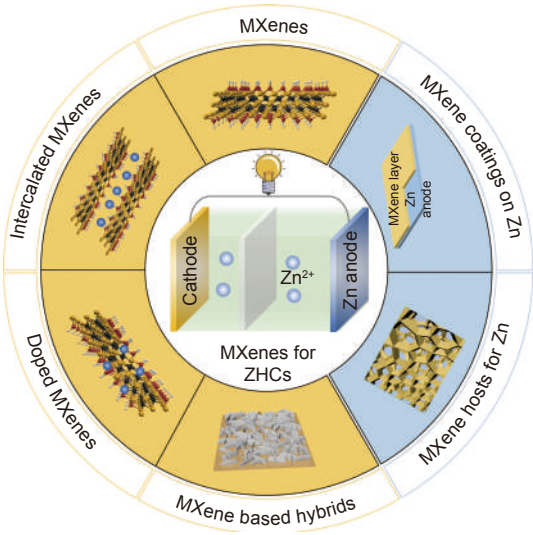

Fig. 2 Schematic diagram of the applications of MXene based nanomaterials for aqueous zinc-ion hybrid capacitors.

spects of MXene based nanomaterials for next-generation ZHCs are briefly discussed.

2 Fundamentals of ZHCs

2.1 Working principles

Basic knowledge about electric double layer (EDL) and pseudocapacitance in supercapacitors (SCs) is presented to facilitate the understanding the working principles of ZHCs. As shown in Fig. 3a, the charge storage mechanism of SCs is mainly reversible accumulation of ions on the electrode surface, specially, a Helmholtz layer can be formed when the electrode is polarized, correspondingly, charge separation occurs at the electrode/electrolyte interface. In order to maintain charge neutrality, electrolyte ions will approach to the surface of the electrode, which results in a diffusion layer. And the above charge adsorption process is named as an EDL mechanism. Therefore, in a typical EDL based SCs, cations and anions are adsorbed on the surface of anodes and cathodes, respectively. Apart from EDL mechanism, pseudocapacitance involves the Faraday charge storage mechanism, which mainly includes redox and intercalation pseudocapacitance (Fig. 3b-c)[43]. Notably, in the case of intercalation pseudocapacitance, the intercalation of ions into the channels or layers of the host materials do not change the crystalline phase of the host materials (Fig. 3c)[44].

A conventional ZHC mainly consists of a battery-type anode as an energy source and an EDL capacitor-type cathode as a power source, which is obviously different from aqueous zinc-ion batteries (ZIBs) with battery cathodes and Zn anodes[44]. As shown in Fig. 3d, a typical ZHC consists of a porous carbon cathode, a Zn anode, and aqueous electrolyte (e.g., $ZnSO_4$, $Zn(CF_3SO_3)_2$, $ZnCl_2$, $Zn(NO_3)_2$)[41, 45], in which Zn^{2+} ions are mainly stored in the surfaces or micropores of the carbon cathode via physical adsorption/desorption of Zn^{2+} ions (similar to the EDL mechanism)[46, 47], and reversible Zn plating/stripping processes occur on the surface of the zinc anode[48]. Furthermore, other zinc storage mechanisms have also been reported in ZHCs, such as chemical adsorption/desorption process[49, 50], and precipitation/dissolution processes of zinc hydroxide sulfate hydrate ($Zn_4SO_4(OH)_6{\cdot}xH_2O$)[40]. Moreover, chemisorption/desorption of Zn^{2+}/H^+ may occur simultaneously in the case of heteroatom-doped carbon cathodes, which may provide additional pseudocapacitance for ZHCs.

Apart from the mentioned type of ZHCs, the second type ZHCs can be constructed with a battery-type cathode with Zn^{2+} ion insertion/extraction reactions and a capacitor-type anode (e.g., active carbon (AC)) with reversible adsorption/desorption of Zn^{2+} ions (Fig. 3e). Although the second type ZHCs can eliminate the use of commercial Zn foil anodes, avoiding the unsolved challenges of zinc metal anodes (e.g., uncontrollable growth of zinc dendrites), many advantages of Zn metal anodes can not be utilized, moreover, few works have focused on this type ZHCs, therefore, the first type ZHCs will be elaborated in the following content, while the second type ZHCs is not included.

2.2 Main electrochemical parameters

Several important parameters are employed to evaluate the overall electrochemical performance of ZHCs, such as capacity/capacitance, energy density, and power density, which will be briefly introduced in this section to better understand the zinc storage mechanisms of ZHCs, and provide guidelines to reas-

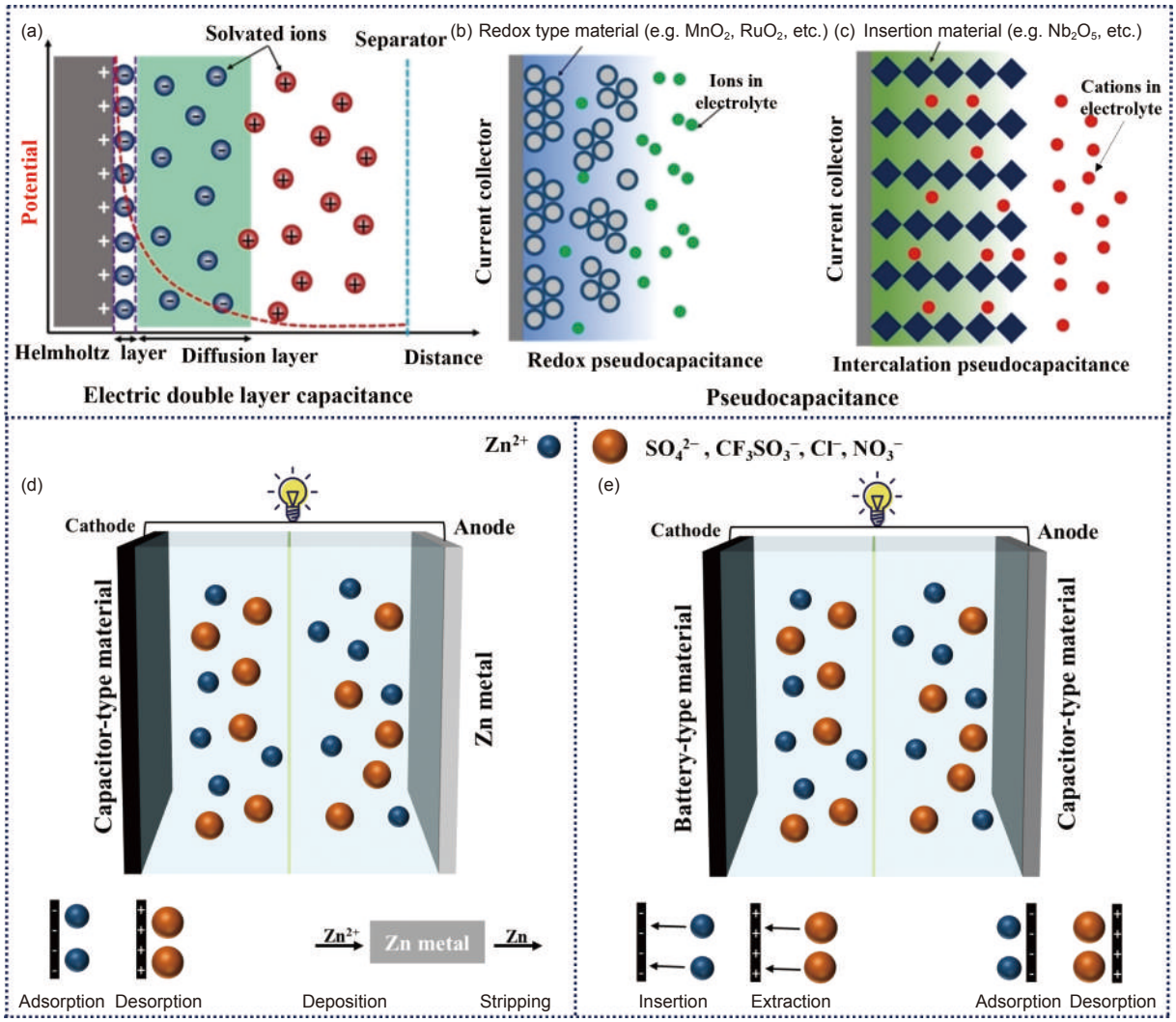

Fig. 3　Schematic of the storage mechanisms of (a) electric double layer capacitance, (b) redox pseudocapacitance, and (c) intercalation pseudocapacitance[44](Reprinted with permission by copyright 2021, Wiley). (d-e) Schematic diagrams of energy storage mechanisms of (d) the first type and (e) the second type ZHCs.

onably evaluate the performance of ZHCs, especially for the beginners in this field. Specific capacitance (C in F g^{-1}), as the most basic parameter, can be calculated by the Equation (1) and (2) [51], in which I, Δt, m, and ΔV represent the discharge current (A), discharge time (s), active material mass (g), and discharge voltage window (V), respectively.

However, for ZHCs containing battery electrodes, capacity (mAh g^{-1}) is also employed to evaluate the electrochemical performance of ZHCs due to the presence of battery electrodes, and capacity may be the appropriate expression especially for two-electrode devices[52]. It is valuable to provide the values of specific capacity of individual electrodes, even for commonly used EDLC materials[53]. For pseudocapacitive materials, the use of capacitance to express performance could avoid obtaining higher-than-theoretical performance[54]. In addition, when potential windows or electrode materials are inconsistent, capacitance values are unreliable for comparison, whereas mAh g^{-1} can be used as a consistent indicator for comparing the properties of different materials[55].

When the charge and discharge curves are linear, the specific capacity (C_m, mAh g^{-1}) is calculated according to Equation (1)[40, 56]:

$$C_m = \frac{I\Delta t}{3.6m} \tag{1}$$

where I is the current (A), Δt is the discharge time (s), and m is the mass of the active material (g).

When the charge and discharge curve are nonlin-

ear, the specific capacity (C_m, mAh g^{-1}) should be calculated by integrating the area under the discharge curve with Equation (2):

$$C_m = \frac{2I\int V\mathrm{d}t}{3.6m\Delta V} \quad (2)$$

The Coulombic efficiency (η) is calculated by Equation (3):

$$\eta = \frac{t_d}{t_c} \quad (3)$$

Where t_d represents the discharge time and t_c represents the charging time.

The energy density (E, Wh kg^{-1}) and power density (P, W kg^{-1}) are calculated according to the following formulas:

$$E = \frac{1}{2}C\Delta V \quad (4)$$

$$P = \frac{3600E}{\Delta t} \quad (5)$$

Where ΔV is the potential window (V).

3 MXenes for cathodes

Compared with hydrophobic porous carbon cathodes in traditional ZHCs, MXenes possess high conductivity and superior hydrophilicity simultaneously, showing promising application in ZHCs with aqueous electrolytes. Further, layered MXenes with large interlayer spacing (~ 1 nm) are favorable for the adsorption of a large number of Zn^{2+}. In addition, the various MXenes with different chemical compositions and functional groups can be doped with heteroatom atoms or composited with other functional nanomaterials, providing great opportunities to reasonably design and construct high-performance MXene-based cathodes for ZHCs[57–59]. In this section, MXene based cathodes will be elaborated with four types of cathodes, which are pure MXenes, intercalated MXenes, heteroatom-doped MXenes, and MXene based hybrids including MXene/metal sulfide hybrids, MXene/carbon hybrids, and MXene/polymer hybrids (Table 1).

3.1 Pure MXenes

MXenes with diverse functional groups possess unique electronic properties. As a new type of 2D materials, MXenes can significantly improve the mechanical stability and speed up the movement of electrons or ions, making it a good choice for electrode materials[71]. Moreover, compared with traditional carbon materials, MXenes not only have excellent electrical conductivity and abundant surface functional groups, but also may make full use of the pseudocapacitance mechanism to store charge. For example, Yang et al.[36] designed a fully degradable and rechargeable Zn-MXene capacitor with electrodeposited zinc nanosheets and Ti_3C_2 MXene as electrodes in the hydrogel electrolyte, and the capacitor exhibited excellent self-discharge resistance. Moreover, the 2D structure and rich surface chemistry of Ti_3C_2 MXene enabled the Zn-MXene capacitor to store Zn^{2+} at high rates, resulting in high capacitance of 132 F g^{-1} at 0.5 A g^{-1} and capacity retention of 82.5% after 1 000 cycles at 3 A g^{-1}. Interestingly, based on the fact that hydrogen peroxide can degrade Ti_3C_2 MXene, Yang et al. designed Zn-MXene capacitors that can be fully degraded by a H_2O_2 induced phosphate buffered saline. The degradable and rechargeable MXene based ZHCs not only increased energy density, but also suppressed the self-discharge of ZHCs, which may provide a new direction to develop degradable and high energy density ZHCs in the future.

MXene nanosheets can be assembled into self-supporting flexible films easily by vacuum filtration. Therefore, the $Mo_{1.33}CT_z$-$Ti_3C_2T_z$ mixed MXene film showed a high capacitance retention of 90% after 8 000 cycles, superior to pure MXene electrodes[60]. Specifically, the CV curves clearly exhibited that the available capacity of pure MXene was far smaller that of the $Mo_{1.33}CT_z$-$Ti_3C_2T_z$. However, agglomeration and restack of MXene nanosheets usually lead to the reduction of exposed active sites for Zn^{2+} storage and long distance transfer for Zn^{2+}[72, 73]. To address the above issues, Li et al.[61] adopted a freeze-casting technique to prepare a 3D porous H-MXene film (3D-PHMF) for ZHCs, in which the introduction of H^+ from HCl solution can effectively alleviate the electrostatic repulsion of MXene nanosheets. As-fabricated 3D-PHMF cathode demonstrated superior zinc storage performance, such as high capacities of 105

Table 1　A summary of various reported MXene based cathodes for ZHCs.

Type of cathode	Sample	Voltage (V)	Electrolyte	Capacity	Capacity retention	Energy density	Power density	Ref.
MXenes	$Ti_3C_2T_x$	0.05-1.35	2 M $ZnSO_4$	132 F g^{-1} at 0.5 A g^{-1}	82.5% after 1000 cycles	–	–	[36]
	$Mo_{1.33}CT_z$-$Ti_3C_2T_z$	0.01-1.3	3 M $Zn(CF_3SO_3)_2$	115 mAh g^{-1} at 1 A g^{-1}	90% after 8000 cycles	103 Wh kg^{-1}	0.143 KW kg^{-1}	[60]
	3D-PHMF	0-1.3	2 M $Zn(CF_3SO_3)_2$	105.6 mAh g^{-1} at 0.2 A g^{-1}	90% after 20000 cycles	53.6 Wh kg^{-1}	104.5W kg^{-1}	[61]
	3DP MXene	0.1-1.2	2 M $ZnSO_4$	259.7 F g^{-1} at 0.1 A g^{-1}	86.5% over 6000 cycles	0.10 mWh cm^{-2}	5.90 mW cm^{-2}	[62]
Intercalated MXenes	$Ti_3C_2T_x$ (Fiber-shaped ZHCs)	0-1.2	1.5 M $ZnSO_4$	214 mF cm^{-2} at 5 mV s^{-1}	83.58% after 5000 cycles	42.8 μWh cm^{-2}	0.64 mW cm^{-2}	[63]
	PDA-MXene	0.2-1.1	2 M $ZnSO_4$	124.4 F g^{-1} at 0.2 A g^{-1}	85% after 10000 cycles	13.8 Wh kg^{-1}	4500 W kg^{-1}	[64]
	In-situ pillared Ti_3C_2	0.2-1.2	0.1 M $ZnSO_4$	73 mAh g^{-1} at 0.2 A g^{-1}	96% after 1000 cycles	–	–	[65]
	Sn^{4+}-Ti_2CT_x/C	0.1-2.0	2 M $ZnSO_4$	138 mAh g^{-1} at 0.1 A g^{-1}	>96% after 12500 cycles	–	–	[33]
Heteroatom-doped MXenes	N-Ti_3C_2	0.05-1.2	1 M $ZnSO_4$	247.9 F g^{-1} at 0.1 A g^{-1}	88.34% after 6000 cycles	45.54 Wh kg^{-1}	4093 W kg^{-1}	[66]
MXene/metal sulfide hybrids	$Ti_3C_2T_x$/ Bi_2S_3@N-C	0-1.4	$ZnSO_4$	653 F g^{-1} at 1 A g^{-1}	85.7% after 2000 cycles	46.98 Wh kg^{-1}	750 W kg^{-1}	[51]
	$Ti_3C_2T_x$/$BiCuS_{2.5}$	0-0.8	1 M $ZnSO_4$	840 C g^{-1} at 1 A g^{-1}	82% after 10000 cycles	298.4 Wh kg^{-1}	7200 W kg^{-1}	[67]
MXene/carbon hybrids	V_2C/CNTs	0.1-1.1	1 M $ZnSO_4$	90.2 F g^{-1} at 10 A g^{-1}	–	–	–	[68]
	MXene-rGO	0.2-1.6	2 M $ZnSO_4$	128.6 F g^{-1} at 0.4 A g^{-1}	95% after 75000 cycles	34.9 Wh kg^{-1}	279.9 W kg^{-1}	[32]
	NMXC	0.2-1.8	2 M $ZnSO_4$	83.9 mAh g^{-1} at 0.1 A g^{-1}	96.4 % after 10000 cycles	64.5 Wh kg^{-1}	3.9 kW kg^{-1}	[34]
MXene/polymer hybrids	MN-80	–	2 M $ZnSO_4$	92.1 mAh g^{-1} at 0.5 mA cm^{-2}	94.31% after 10000 cycles	–	–	[35]
	MXene/BCF	0-1.2	2 M $Zn(CF_3SO_3)_2$/PAM gel	178.6 mF cm^{-2} at 0.5 mA cm^{-2}	72.3% after 3000 cycles	34.0 μWh cm^{-2}	–	[69]
	MXene/BC@PPy	0-1.9	2 M $Zn(CF_3SO_3)_2$-0.1 M $MnSO_4$/PAMhydrogel	388 mF cm^{-2} at 1 mA cm^{-2}	95.8% after 25000 cycles	145.4 μWh cm^{-2}	3.78 mW cm^{-2}	[70]

Note: M: mol L^{-1}

and 62.7 mAh g^{-1} at 0.2 and 5 A g^{-1}, respectively. Taking advantage of the easy assembly of MXene nanosheets, high-mass-loading MXene based electrodes can be expected to achieve high-energy-density ZHCs.

MXene nanosheets with negatively charge surface possess outstanding hydrophilicity, facilitating the formation of stable ink[74]. As a typical example, the MXene gel ink was firstly obtained through a general divalent cation (M^{2+}) assisted gelation strategy, in which a small amount of M^{2+} (e.g., Zn^{2+}) acted as effective cross-linkers to enhance the interaction between MXene nanosheets (Fig. 4a-b)[62]. Zn^{2+} gelled MXene nanosheets provided multi-dimensional Zn^{2+} diffusion paths, and abundant voids, ensuring the easy penetration of electrolytes. Therefore, 3D printed (3DP) MXene electrodes enabled the corresponding ZHCs with a high capacitance of 184.4 F g^{-1} at 10 A g^{-1} (Fig. 4c). Notably, the 3DP electrodes possessed highly interconnected frameworks, customizable mass loading and capacitances, meanwhile, 3DP also facilitated the construction of high-mass-loading electrodes for high-energy-density ZHCs, thus 3DP would be a promising choice for high-performance ZHCs in consumer electronics.

With the thriving development of wearable electronics, flexible energy storage devices are requested to exhibit excellent flexibility[75, 76]. To this end, Shen et al.[63] fabricated fiber-shaped ZHCs by braiding shell zinc fibers anode on the surface of $Ti_3C_2T_x$ fibers core cathode, forming an ultralong tubular structure with excellent flexibility. Most importantly, the shape of CV curves under different curvature diameters were well maintained, correspondingly, 95% of its original capacitance was recorded in the case of twisted (180°) counterparts. This work provides a direction for the mass production and practical applications of wearable energy storage devices.

Despite the great progress of MXenes for ZHCs, the construction of high-performance MXene cathodes is still in its infancy since the influence of thickness and functional groups of $Ti_3C_2T_x$ nanosheets in zinc storage performance is still elusive, and other type MXene nanosheets (e.g., Nb_2CT_x) are rarely employed for ZHCs, because Nb_2CT_x exhibited different electrochemical properties under different scanning

voltage windows[77]. Therefore, MXene cathodes still provide many opportunities for high-performance ZHCs.

3.2 Intercalated MXenes

MXenes with expanded interlayer spaces can provide more zinc storage sites, shorten the diffusion distance of zinc ions and greatly facilitate zinc intercalation kinetics, thus intercalated MXene cathodes usually exhibit superior electrochemical performance to traditional MXene counterparts. Organic molecules are frequently employed to intercalate into MXenes, in which electrostatic attraction between negatively charged MXene hosts and positively charged guests plays a key role during the intercalation process. As a typical example, Peng et al.[64] used small organic diamine molecules to precisely control the interlayer spacing of MXene (Fig. 4d-e). Ethylenediamine (EDA), 1, 3-propylenediamine (PrDA), 1, 4-butylenediamine (BDA) and *p*-phenylenediamine (PDA) can interact with oxygen-containing functional groups on the surface of MXene to form the wrinkled MXene surface and 3D porous architecture, which can effectively avoid the agglomeration of MXene nanosheets. Because the expanded interlayer spacing enabled by the intercalated PDA molecules matched the size of Zn^{2+} ions best, the PDA intercalated MXene cathode showed the best electrochemical stability and cycling life among MXene and all the intercalated MXenes with diamine molecules (Fig. 4f), as confirmed by a high capacitance of 84.4 F g^{-1} at 10 A g^{-1} and a capacitance retention of 85% after 10 000 cycles at 1 A g^{-1} (Fig. 4g). Moreover, Philip et al.[65] adopted an in-situ pillaring method by dissolving surfactants (hexadecyltrimethy-lammonium bromide, CTAB) in the electrolyte and inserted them into Ti_3C_2 MXene, correspondingly, the interlayer spacing could be increased from 0.15 to 0.55 nm, greatly facilitating zinc storage performance, as evidenced by an average capacity of 86 mAh g^{-1} at 20 mA g^{-1} and a high capacity retention of 96% after 1 000 cycles at 0.2 A g^{-1}. In this regard, the layer spacing of MXene can be precisely controlled by rationally selecting suitable organic mo-

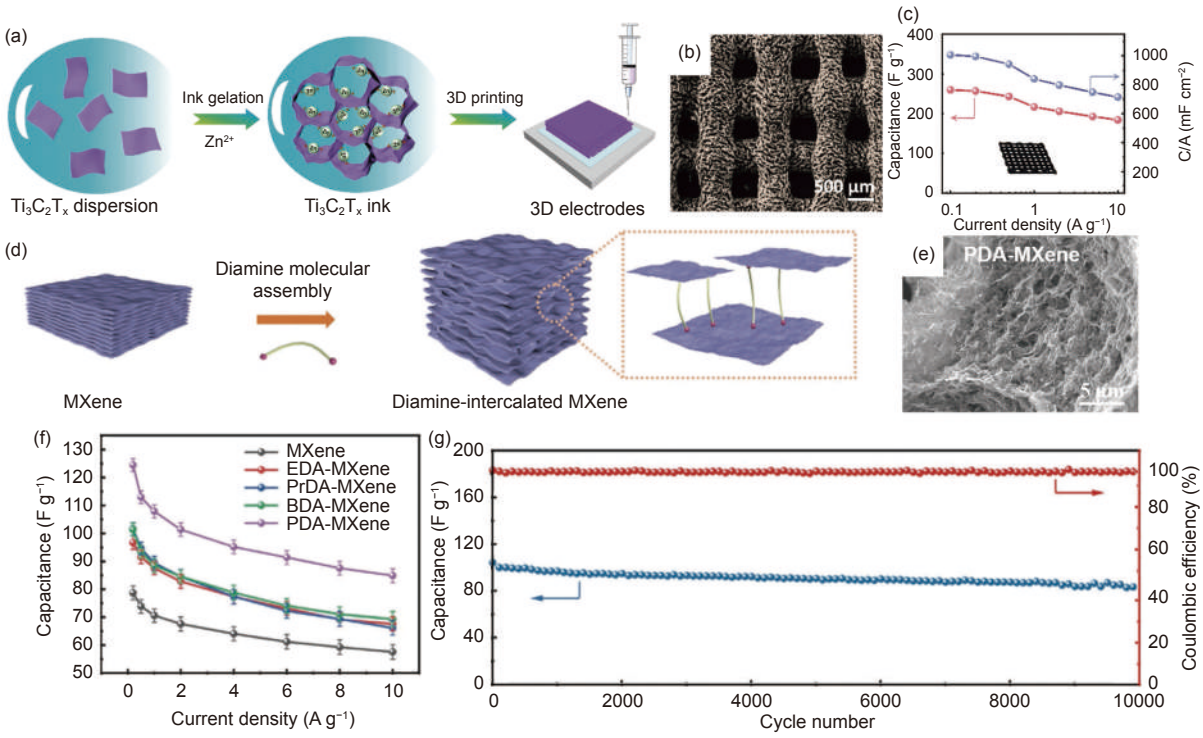

Fig. 4 (a) Schematic diagram of 3DP MXene electrodes. (b) SEM image of 3DP MXene. (c) Specific capacitances based on mass and area at different current densities[62](Reprinted with permission by copyright 2021, ACS). (d) Schematic diagram of the preparation process of diamine-intercalated MXene. (e) SEM image of PDA-MXene. (f) Specific capacitances of MXene electrodes intercalated with different diamine molecules at different current densities. (g) Cycling performance of PDA-MXene electrodes at 1 A g^{-1}[64](Reprinted with permission by copyright 2021, Wiley).

lecules with different sizes, correspondingly, the zinc storage performance of MXene cathodes can be effectively optimized.

Apart from organic molecules, metal ions are also frequently employed as the intercalation species. For example, Sn^{4+} ions were intercalated into Ti_2CT_x MXene (Sn^{4+}-Ti_2CT_x/C), and the interlayer spacing of Ti_2C MXene was expanded from 1.15 to 1.27 nm, and the specific surface area was increased from 6.1 to 6.4 $m^2\ g^{-1}$[33]. Correspondingly, the specific discharge capacitance of the Sn^{4+}-Ti_2CT_x/C based ZHCs was 138 and 92 mAh g^{-1} at 0.1 and 5.0 A g^{-1}, respectively, obviously higher than the values of Ti_2AlC/C and core-shell Ti_2CT_x/C sphere electrodes. Moreover, Sn^{4+}-Ti_2CT_x/C also displayed a long lifespan up to 12 500 cycles at 0.5 A g^{-1}, superior to Ti_2AlC/C and Ti_2CT_x/C counterparts. With the consideration of various metal cations with different radius (e.g., Zn^{2+}, Cu^{2+}, K^+), such interlayer engineering by metal cation intercalation may pave the way to tune electrochemical performance of MXene based ZHCs.

3.3 Heteroatom-doped MXenes

It is well known that heteroatoms (e.g., N, S) can provide more active sites for MXenes, and these heteroatoms can effectively tune the band structures of MXenes for enhanced conductivity[78]. Moreover, the introduction of heteroatoms (e.g., N) increases the interlayer repulsion, which greatly inhibits the aggregation of MXene nanosheets and improves the structural stability of MXene cathodes during cycling. For example, Jin et al.[66] synthesized a N-doped Ti_3C_2 (N-Ti_3C_2) with a N element content of 3.3 at.% by a hydrothermal method using urea as a nitrogen source. Owing to the additional pseudocapacitance generated by the redox of pyrrolic nitrogen, the cyclic voltammetry (CV) curve of N-Ti_3C_2 had a distinct hump at 10 mV s^{-1}, while, in the case of Ti_3C_2 electrode, no peak could be found. The advantages of N doping were mainly reflected in its electrochemical performance. As a result, the N-Ti_3C_2 electrode achieved a long cycle life of 6 000 cycles at 1.5 A g^{-1}, and a high capacitance retention of 88.34% after 1 000 cycles, which is higher than the value of Ti_3C_2 electrode (78.12%). Other type heteroatom doped MXenes are highly needed to develop and evaluate their zinc storage performance. Moreover, a synergistic effect may be expected in the case of heteroatom co-doped MXene cathodes for enhanced electrochemical performance with new storage mechanisms. The key is to develop new strategies to controllably synthesize desirable heteroatom co-doped MXene materials.

3.4 MXene based hybrids

As mentioned above, MXenes have excellent conductivity, hydrophilicity, unique 2D structure and chemical composition, thus conductive MXene nanosheets can serve as ideal substrates for electrochemical active material loading for improved conductivity. The combination of MXenes with other high capacitance materials can not only prevent the self-stacking of MXene nanosheets, but also improve the electrical conductivity of the hybrid electrodes. In this section, MXene-based hybrids are classified into three parts in terms of the types of active materials, which are MXene/metal sulfide hybrids, MXene/carbon hybrids, and MXene/polymer hybrids.

3.4.1 MXene/metal sulfide hybrids

Metal sulfides usually possess poor conductivity, the presence of MXene can effectively accelerate the electron transport in MXene/metal sulfide hybrid electrodes, meanwhile, MXene nanosheets can prevent the agglomeration of metal sulfide particles to improve their utilization rate in high-capacity ZHCs. For instance, Zhang et al.[51] successfully prepared a ternary N-doped carbon wrapped Bi_2S_3 intercalated $Ti_3C_2T_x$ ($Ti_3C_2T_x$/Bi_2S_3@N-C) with a pizza-like heterostructure by an in-situ growth and calcination. With the help of the dopamine derived N doped carbon (N-C) membrane, $Ti_3C_2T_x$ and Bi_2S_3 could be better combined and the internal resistance was effectively reduced, thus $Ti_3C_2T_x$/Bi_2S_3@N-C electrodes achieved excellent electrochemical performance, such as high a power/energy density of 750 W kg^{-1}/46.98 Wh kg^{-1}, and a remarkable capacitance retention of 85% after 2 000 cycles.

Further, Li et al.[67] adopted an in-situ deposition and "baton relay" method to obtain a $Ti_3C_2T_x$/$BiCuS_{2.5}$

hybrid electrode (Fig. 5a). Interestingly, when the ratio of Bi to Cu reached 1∶1, the bimetallic sulfide showed a layered structure, thus the specific capacity and the oxidation/reduction reaction kinetics were greatly increased. Notably, the synergistic effect in the $Ti_3C_2T_x$/$BiCuS_{2.5}$ with strong interactive interface effectively accelerated the ion transport rate. As shown in Fig. 5b, the $Ti_3C_2T_x$/$BiCuS_{2.5}$ cathodes showed an energy/power density of 298.4 Wh kg^{-1}/7.2 kW kg^{-1} and a high capacity retention of 82% after 10 000 cycles (Fig. 5c), demonstrating their excellent zinc storage performance. In this regard, other metal sulfides are expected to exhibit high performance in their corresponding ZHCs.

3.4.2 MXene/carbon hybrids

Various carbon nanomaterials are reported to be composited with MXene nanosheets to prepare MXene/carbon hybrids, in which the presence of carbon nanomaterials can provide abundant zinc storage sites and prevent the stack of MXene nanosheets for high-capacity ZHCs, and 2D MXene nanosheets effectively facilitate fast electron transfer between adjacent carbon particles. As a typical example, Wang et al.[68] used V_2C MXene and carbon nanotubes (CNTs) as raw materials to prepare a composite material with a cross-staking structure (V_2C/CNTs) (Fig. 6a-b). The successful introduction of carbon nanosheets can largely prevent the self-stacking of V_2C MXene, form excellent conductive networks, and improve the interlayer accessibility of V_2C. Thus, the multilayer porous V_2C MXene exhibited a high specific capacitance of 90.2 F g^{-1} at 10 A g^{-1}, and the Coulombic efficiency approached to 100% after 4 000 cycles, showing the excellent stability and rate performance. Notably, X-ray absorption fine structure (XAFS) characterization showed that the K-edge spectrum of Zn did not change much within the voltage window of 0.1-1.1 V, indicating that the $(Zn(OH)_2)_3(ZnSO_4)(H_2O)_n$ was always deposited on the cathode. Further observation indicated that the precipitate flakes on the cathode of V_2C/CNTs had a more regular shape and larger flakes at a discharge voltage of 0.1 V than the counterpart at 0.5 V.

Not limited to CNTs, graphene nanosheets were also employed to composite with MXenes. For example, Wang et al.[32] prepared reduced graphene ox-

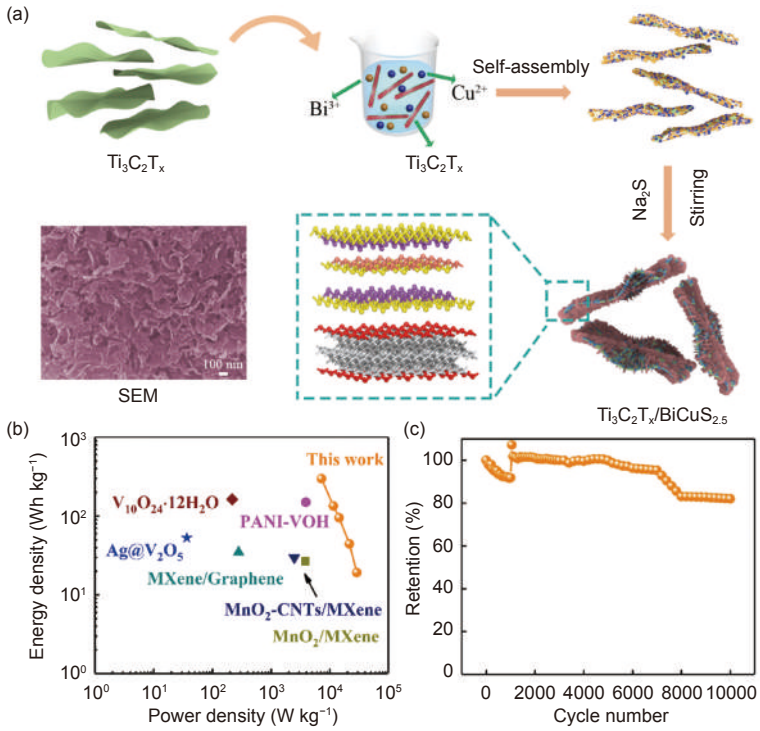

Fig. 5 (a) Schematic diagram of preparation of $Ti_3C_2T_x$/$BiCuS_{2.5}$. (b) Ragone plot of $Ti_3C_2T_x$/$BiCuS_{2.5}$ and other reported electrodes. (c) Cycling performance of $Ti_3C_2T_x$/$BiCuS_{2.5}$ electrodes at a current density of 20 A g^{-1}[67](Reprinted with permission by copyright 2021, Elsevier).

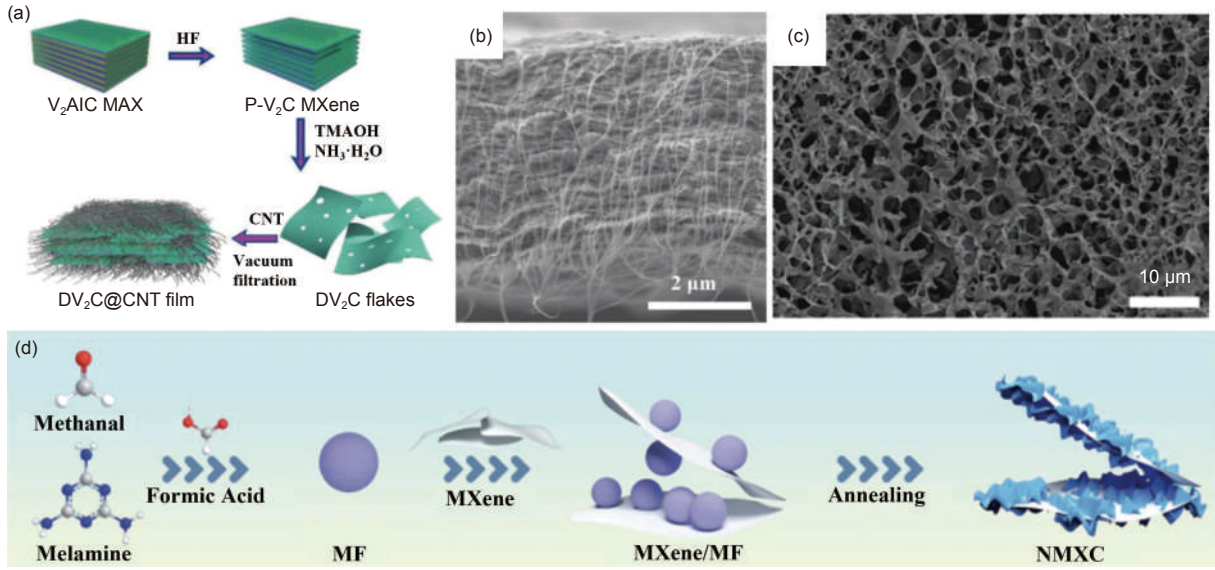

Fig. 6　(a) Schematic of the synthesis of V_2C@CNTs. (b) SEM image of V_2C@CNTs[68](Reprinted with permission by copyright 2019, Wiley). (c) SEM image of MXene-rGO[32] (Reprinted with permission by copyright 2019, Wiley). (d) Schematic of the synthesis of NMXC[34] (Reprinted with permission by copyright 2021, RSC).

ide (rGO) aerogels by a hydrothermal and freeze-drying process, subsequently, porous MXene-rGO aerogels (Fig. 6c) with excellent conductivity and hydrophilicity were synthesized by the similar synthesis route to rGO aerogels. Moreover, MXene-rGO can eliminate the usage of conductive additives. Importantly, the CV area of MXene-rGO cathode was larger than that of rGO electrode. Meanwhile, MXene-rGO cathode delivered a specific capacitance of 128.6 F g^{-1} at 0.4 A g^{-1} and an energy/power density of 34.9 Wh kg^{-1}/279.9 W kg^{-1}. In addition, the capacitance retention was as high as 95% after 75 000 cycles at 5 A g^{-1}.

Further, N-doped MXene coated by N-doped amorphous carbon (NMXC) was developed through the self-assembly of melamine formaldehyde microspheres (MF) and MXene and subsequent calcination processes (Fig. 6d)[34]. The MF microspheres could be electrostatically adsorbed on the surface of MXene. After pyrolysis, a wrinkled N-doped MXene based heterostructure was obtained, in which the formed carbon layers could prevent MXene from being oxidized at high potential, and the wrinkled porous frameworks could ensure a high specific surface area of 143.3 m^2 g^{-1}. Based on the above advantages, the Zn//NMXC ZHSCs achieved a high capacity retention of 87.1% after 9 000 cycles at 5 A g^{-1}. This work may shed light on the rational construction of MXene-based cathodes for high-performance ZHCs.

3.4.3　MXene/polymer hybrids

Synergistic effects can also be expected in MXene/polymer hybrid cathodes. For example, Chen et al.[35] first modified $Ti_3C_2T_x$ by an alkalization and post-rolling method to effectively reduce the —F and —OH functional groups to decrease active sites. The mechanical properties of $Ti_3C_2T_x$ can be significantly enhanced by the combination of the soybean stack derived nanofibrous cell (NFC). Moreover, the NFC as the support of $Ti_3C_2T_x$ can greatly alleviate the stacking problem of $Ti_3C_2T_x$, and optimize the mechanical and electrochemical properties. ZHC was assembled with zinc foil as the anode, $Ti_3C_2T_x$ composite film with a mass percentage of 80% (MN-80) as the cathode and $ZnSO_4$ as the electrolyte, which maintained a high-capacity retention of 94.31% after 10 000 cycles at 8 mA cm^{-2} in charge and discharge tests, showing excellent cycle stability. This study provides guidance for the applications of high-performance electrodes.

In addition, the uniform insertion of polymer will increase the layer spacing between MXene sheets and accelerate the transfer rate of ions. Therefore, Cao et

al.[69] used the vacuum assisted self-assembly method to evenly insert bacterial cellulose fibers (BCFs) into MXene nanosheets to prepare MXene/BCF hybrid films with larger layer spacing than pure MXene. The transfer kinetics of Zn^{2+} on the MXene/BCF hybrid film electrode was faster than that of the pure MXene film electrode. With the advantage of significantly reduced electrostatic barrier, Zn^{2+} can be intercalated quickly and reversibly in MXene, significantly improving the rate performance and cycle stability of Zn-ion micro-supercapacitors (ZMSCs). Compared with pure MXene, MXene/BCF showed a higher areal capacitance, indicating that MXene/BCF has a better charge storage capacity. After 3 000 cycles, the capacitance retention of the hybrid film could reach 71.8%, 2.5 times as much as that of pure MXene film. With the voltage window of 0-1.2 V, the CV curve of the MXene/BCF hybrid film electrode was more rectangular than that of pure MXene, indicating better electrochemical reversibility. It is worth noting that the MXene/BCF hybrid electrode can well suppress the generation kinetics of hydrogen/oxygen, resulting in a high working voltage of ZMSCs.

Furthermore, Cheng et al.[70] polymerized pyrrole monomers (PPy) on the surface of 1D bacterial cellulose (BC) nanofibers through chemical oxidation to prepare BC@PPy hybrids, which were evenly inserted into $Ti_3C_2T_x$ nanosheets to prepare MXene/BC@PPy hybrid films. Specifically, BC@PPy, as an electrically active material, improved the storage capacity of charge. At a current density of 1 mA cm^{-2}, the MXene/BC@PPy based ZMSCs showed an areal capacitance 388 mF cm^{-2}, which is 10 times that of the pure MXene film electrode. After 25 000 cycles, the capacitance retention was as high as 95.8%. In order to meet the requirements of wearable electronic products, ZMSCs were further combined with liquid metal to realize a scalable ZMSC array, notably, a capacitance retention rate of 90.6% was still achieved after 18 000 cycles, during which the ZMSC array was stretched with an elongation rate of 400 % every 200 cycles. This research provides a new technique to construct stretchable ZHCs for wearable microelectronics.

4 MXenes for Zn anodes

Generally, zinc metal can be directly used as the anode for ZHCs because of its suitable potential and high hydrogen evolution overpotential. However, non-uniform electrical field and Zn^{2+} ion flux usually leads to random nucleation and uncontrollable growth of zinc dendrites, which may pierce through the separator and result in the failure of ZHCs[79–81]. In this regard, the emerging MXene nanosheets can physically guide Zn^{2+} ion flux by the unique 2D nanostructure, and induce uniform nucleation and growth of Zn due to the zincophilic surface of MXene nanosheets. Therefore, the presence of MXenes can greatly suppress Zn dendrites and prolong the cycling life of ZHCs. In this section, the applications of MXenes in the anodes of ZHCs are divided into MXene hosts for Zn and MXene coating for Zn in terms of the functionalities and roles of MXene nanosheets (Table 2).

4.1 MXene hosts for Zn

When MXene nanosheets serve as Zn hosts, the conductive MXene nanosheets provide fast electron transfer pathways in 2D directions, and the abundant functional groups on MXene can act as zincophilic sites to induce uniform zinc deposition. Further, MXene nanosheets can be assembled into 3D porous networks with high pore volume by hydrothermal or metal cation induced assembly strategies[85–89], providing sufficient space to accommodate deposited Zn.

Flexible $Ti_3C_2T_x$ MXene can be made from the $Ti_3C_2T_x$ colloidal solution without any additives, and as-synthesized $Ti_3C_2T_x$ MXene possesses high electrical conductivity (15 100 S cm^{-1}), mechanically flexible and environmentally friendly, which makes it a promising candidate for metal current collectors and ideal hosts for zinc metal to construct high energy density ZHCs[90]. Tian et al.[37] prepared advanced $Ti_3C_2T_x$ MXene@Zn anodes with 3D lamination by deposition of Zn nanosheets on $Ti_3C_2T_x$ MXene, which effectively prevented the growth of Zn dendrites by virtue of its excellent hydrophilic and mechanical properties (Fig. 7a). Therefore, Zn plating/strip-

Table 2　A summary of various reported MXene-based anodes for ZHCs.

Role of MXenes	Anode name	Voltage hysteresis	Nucleation overpotential	Life span	Coulombic efficiency	Ref.
Zn host materials	$Ti_3C_2T_x$ MXene@Zn	75 mV(1 mA cm^{-2})	83 mV	300 h(1 mA cm^{-2})	94.13% at 5 mA cm^{-2} (400 cycles)	[37]
	MCl-Zn	103 mV(10 mA cm^{-2})	40.7 mV(1 mA cm^{-2})	840 h(2 mA cm^{-2})	99.50% at 1 mA cm^{-2} (50 cycles)	[82]
	MGA@Zn	64 mV(10 mA cm^{-2})	–	1050 h(10 mA cm^{-2})	≈99.67% at 10 mA cm^{-2} (600 cycles)	[83]
Protecting layers	S/MX@ZnS@Zn-350	0.03 V(0.5 mA cm^{-2})	–	1600 h(10 mA cm^{-2})	–	[38]
	MXene-mPPy/Zn	22 mV(0.2 mA cm^{-2})	10 mV	2500 h(0.2 mA cm^{-2})	–	[84]
	AMX-Zn	–	–	–	–	[81]
	MXene@Zn (Zn-p)	30 mV(1 mA cm^{-2})	27.4 mV(1 mA cm^{-2})	200 h (1 mA cm^{-2})	–	[31]

ping process was stable after 50 cycles and showed better cycling stability and Coulombic efficiency over 400 cycles than bare pure Zn (Fig. 7b), which could be ascribed to the stable and compatible interface between $Ti_3C_2T_x$ and Zn.

During the deposition process of Zn, the Zn^{2+} ions firstly interact with the outermost layer of MXene rather than the inner transition metal layer[91]. However, the underlying subtle mechanisms involving lattice matching and surface termination induction remain a challenge due to limited synthesis strategies of MXene nanosheets with desirable termination. Recently, Li et al.[82] synthesized halogenated MXenes ($Ti_3C_2Cl_2$, $Ti_3C_2Br_2$, and $Ti_3C_2I_2$) by a copper halide based molten salt etching approach. Due to the joint action of halogen terminal adjustment and high lattice matching between MXene and Zn, the uniform nucleation and growth of zinc on the MXene crystal plane was guaranteed, effectively avoiding the formation of zinc dendrites. Importantly, $Ti_3C_2Cl_2$-Zn exhibited excellent cyclic stability and fast redox kinetics as indicated by the lowest polarization voltage of 103 mV. Impressively, the MXene modified zinc anode could operate for 9 000 cycles (Fig. 7c).

With the consideration of degradable ZHCs for environmental protection, Yang et al.[36] firstly used the constant voltage deposition technology to vertically deposit Zn nanosheets on Ti_3C_2 films. When as-fabricated Zn-MXene hybrid anode was immersed in a phosphate buffered saline (PBS) triggered by medical H_2O_2 at 85 °C, it could be degraded within 4 days, obviously shorter than the commercial Zn foils (30 days). Notably, part of the Zn nanoflakes were converted into Zn containing inorganic salts, and when the immersion time was prolonged to 7 days, the Zn nanosheets completely disappeared. Importantly, the electrochemical performance of the ZHCs assembled with the MXene film cathode and Zn-MXene hybrid anode was almost the same regardless of its bending angels of 0° and 180°. This work may trigger the development of fully degradable ZHCs in the future.

Further, MXene nanosheets can be assembled into 3D porous networks with high pore volume[85–89], providing sufficient space for Zn deposition. As a typical example, MXene and graphene nanosheets were hydrothermally assembled into a bendable aerogel (MGA), and MGA can be employed as Zn host materials[83], in which bulk Zn was firmly anchored within MGA by one-step electrodeposition for MGA@Zn hybrid anodes. Interestingly, the ZnF_2-rich surface could be in-situ generated by the reaction of the F-containing functional groups on MXene nanosheets with primally deposited Zn, which tremendously promoted the diffusion kinetics of Zn^{2+} ions, avoiding the occurrence of side reactions due to the non-contact between Zn and the electrolyte. Consequently, the corrosion potential of Zn in MGA@Zn hybrid electrodes increased from −0.988 to −0.961 V. Compared with the Cu@Zn electrode, the surface of the MGA@Zn anode was relatively flatter. Therefore, in contrast to commercial Zn foil anodes with limited surface area, the MXene/Zn hybrid anodes may possess rough surface or high specific area, thus high-rate ZHCs with high power density can be expected in such MXene/Zn hybrid anodes.

4.2　MXene coatings on Zn

MXene nanosheets can be assembled into 2D films on Zn anodes. The presence of MXene-based coating layers plays unique roles in suppressing zinc dendrites by homogenizing Zn^{2+} ion flux and local

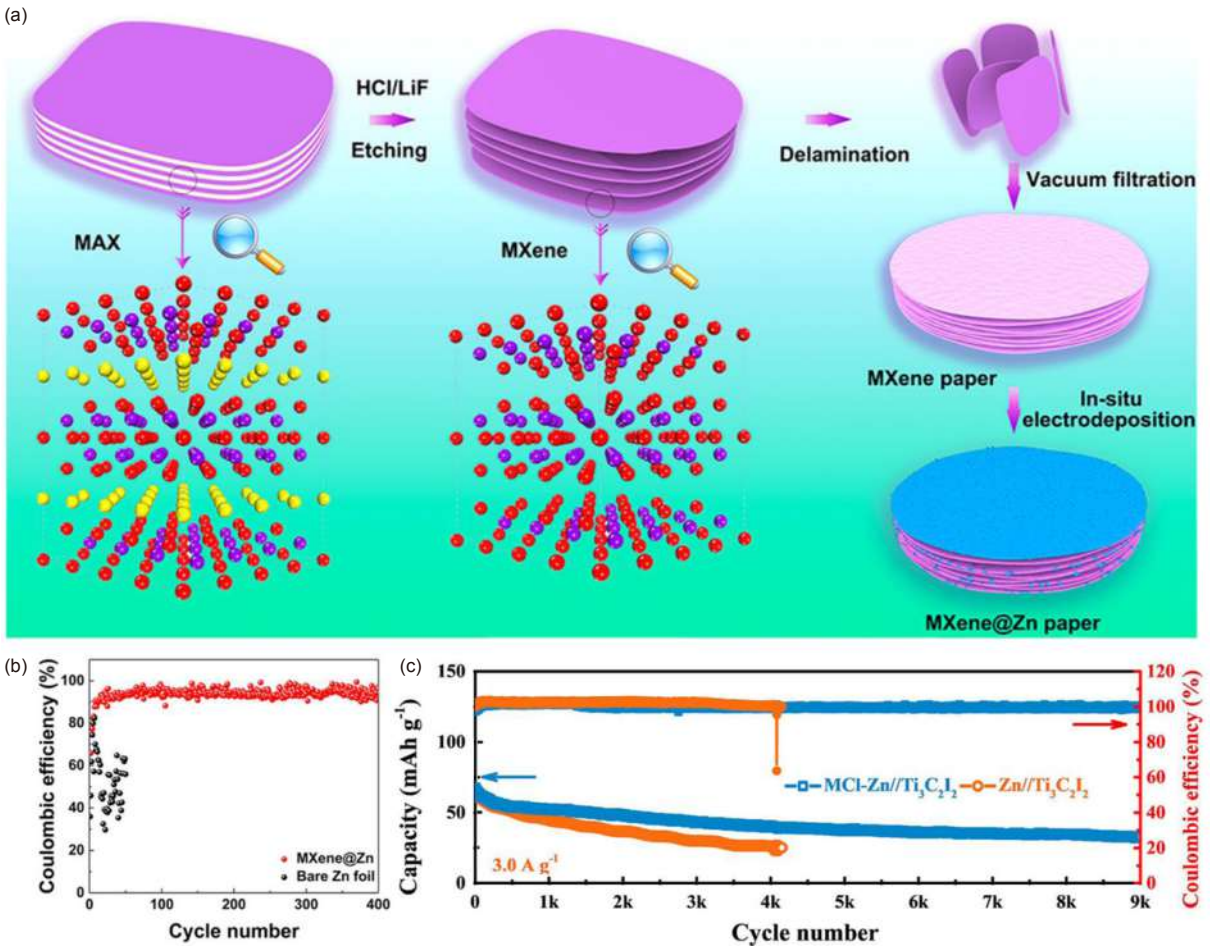

Fig. 7 (a) Schematic diagram of the preparation of a flexible layered $Ti_3C_2T_x$ MXene@Zn paper. (b) Coulombic efficiency of Zn plating/stripping of Zn|Ti@Zn batteries and Zn|MXene@Zn batteries at an areal capacity of 1 mAh cm^{-2} and a current density of 1 mA cm^{-2}[37](Reprinted with permission by copyright 2021, ACS). (c) Cycling performance of Zn//$Ti_3C_2I_2$ and MCl-Zn//$Ti_3C_2I_2$ batteries at a current density of 3 A g^{-1}[82]. (Reprinted with permission by copyright 2022, ACS).

electric field for uniform zinc deposition, meanwhile, low polarization voltages are usually achieved due to the high conductivity of MXenes. Moreover, MXene can also reduce the deformation of zinc anodes and improve the utilization rate of zinc, thus improving the cycle stability and Coulombic efficiency of Zn anodes. As a typical example, An et al.[38] used a protective layer consisting of S-doped MXene frameworks and ionic conductive ZnS on Zn anode (S/MX@ZnS@Zn) to induce uniform growth of Zn nanosheets (Fig. 8a). Specifically, ZnS on the Zn surface effectively avoided the occurrence of side reactions, and accelerated the ion migration ability to induce uniform deposition of zinc. Meanwhile, S-doped 3D MXene could distribute electric field uniformly, reduce local current density and adapt to volume changes during plating and stripping cycles. Compared with the Zn||Zn battery with a pristine Zn anode with alarge polarization voltage of 0.145 V and a short cycle lifetime of 545 h at 0.5 mA cm^{-2}, the S/MX@ZnS@Zn electrodes treated at 300 and 350 °C, which were labeled as S/MX@ZnS@Zn-300 and S/MX@ZnS@Zn-350, respectively, exhibited a low polarization voltage of about 0.030 V and a long cycling life of 1 600 h (Fig. 8b). The superior electrochemical performance was further confirmed by the smooth surface of the cycled S/MX@ZnS@Zn-350 anode (Fig. 8c), indicating the unique roles of MXene nanosheets in suppressing Zn dendrites.

Apart from pure MXene materials, MXene-based hybrids are also good choices to serve as Zn coating layers. For instance, Zhang et al[84] employed a

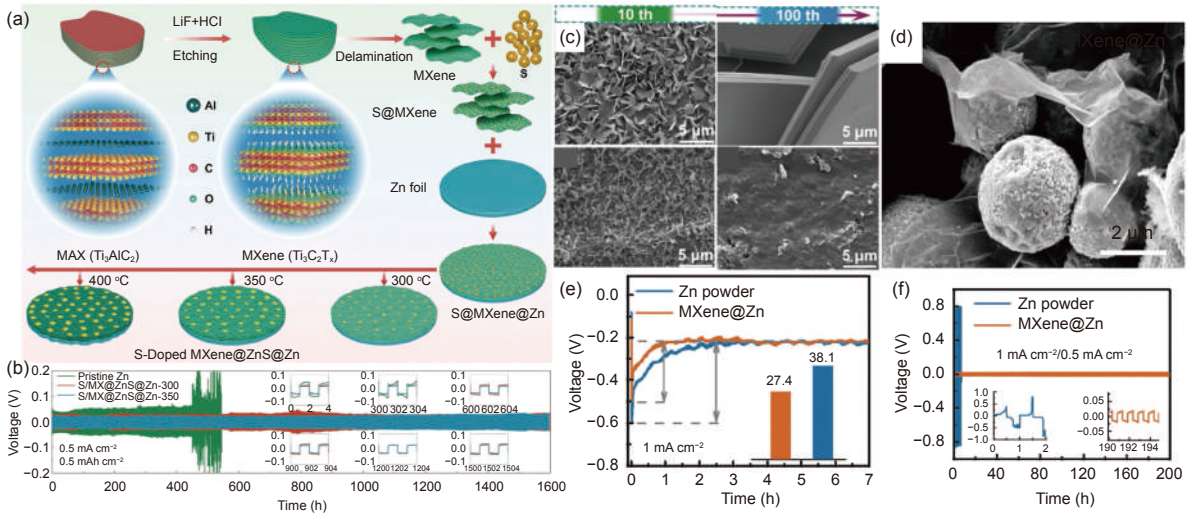

Fig. 8　(a) Schematic of the synthesis of S/MX@ZnS@Zn. (b) Cycling performance of pristine Zn and S/MX@ZnS@Zn anodes at a rate of 0.5 mA cm^{-2} and an areal capacity of 0.5 mAh cm^{-2}. SEM images of (c) pristine Zn anodes and S/MX@ZnS@Zn-350 anodes after 10 and 100 cycles[38] (Reprinted with permission by copyright 2021, ACS). (d) SEM image of MXene@Zn. (e) Nucleation overpotential of Zn-p and MXene@Zn at 1mA cm^{-2}. (f) Long-cycle performance diagram of Zn-p and MXene@Zn symmetric batteries at 1 mA cm^{-2}[39](Reprinted with permission by copyright 2021, ACS).

MXene-based mesoporous polypyrrole layer (MXene-mPPy) to spray on Zn foil (MXene-mPPy/Zn), and the MXene-mPPy/Zn cell outstandingly ran over 2 500 h at 0.2 for 0.2 mAh cm^{-2}, far exceeding the cell with the polypyrrole sprayed Zn foil (PPy/Zn) and pure Zn foil. Meanwhile, the MXene-mPPy layer possessed flat and smooth surface.

Alkalized MXene (AMX) was also reported to composite with Zn for AMX-Zn hybrid anodes[81]. Specially, a 3D metal/MXene derived composite material with a nanoribbon structure was synthesized through an alkalization and metal ion pre-intercalation strategy. The corresponding ZHCs exhibited a high capacitance retention of 92.5% after 10 000 cycles at 3.3 A g^{-1} and a high energy density of 21.08 Wh kg^{-1} at a power density of 7.04 kW kg^{-1}. Moreover, uniform Zn nanosheets were deposited on the surface of the AMX-Zn anode, and no obvious Zn dendrites could be observed, indicating that MXene-derived materials offered abundant active sites and ion transport channels.

In contrast to Zn foils, Zn powder (Zn-p) stands out because of its cheap price and easy processing. Different from the conventional short circuit behavior of Zn foils due to the growth and accumulation of Zn dendrites, Zn-p failure is related to the rapid deterioration of overpotential, which could be addressed by $Ti_3C_2T_x$ MXene. Specifically, $Ti_3C_2T_x$ MXene-wrapped zinc powder (MXene@Zn) anodes were prepared by a self-assembly method (Fig. 8d)[31]. Compared with Zn foil batteries with overpotentials up to 83 mV, the Zn-p||Zn-p and MXene@Zn||MXene@Zn cells exhibited reduced overpotentials of 38.1 and 27.4 mV at 1 mA cm^{-2} (Fig. 8e), respectively. Meanwhile, the MXene@Zn anode exhibited a small overpotential of 30 mV at 1 mA cm^{-2} and a lifetime of 200 h (Fig. 8f). This work provides new insights into the potential application of Zn-p anodes in practical zinc-based energy storage devices.

5　Conclusions and prospects

ZHCs well integrate high energy density of ZIBs with high power density of supercapacitors, and have become a type of promising energy storage devices. However, traditional porous carbon cathodes and commercial Zn foil anodes are faced with low capacity and limited cycling life, respectively. As a new type of 2D materials with a unique layered structure, MXenes have been gradually used as electrodes of ZHCs due to their excellent conductivity and hydrophilicity. This paper systematically reviews the recent progress of MXene-based nanomaterials in cathodes and Zn anodes of ZHCs. Despite the great progress of

MXene electrodes for ZHCs, some challenges and issues are still unsolved.

(1) The stability of MXene during its ZHC application. MXene products especially for ultrathin MXene nanosheets tend to be oxidized during their storage and charge/discharge cycles, which mainly origins from the easy oxidation of the intrinsic surface functional groups (—O, or —F) on MXene by dissolved oxygen in the dispersed solution (e.g., H_2O)[92, 93]. The deterioration of MXene quality seriously degrades its excellent conductivity and leads to capacity decay of corresponding ZHCs. Recent study indicates that hydration chemistry of inorganic salts enabled the storage life of MXene up to 400 days, which may provide a feasible way to use MXenes in ZHCs without their degradation concerns[94].

(2) Controllable synthesis of MXenes with suitable structures and terminal groups for MXene-based cathodes. Pure MXenes deliver low capacity due to their high molecular weight and limited zinc storage sites. One effective strategy to improve the zinc storage performance is to introduce electrochemical active functional groups on MXenes, which require the new and controllable synthesis of MXenes. And molten salt synthesis of MXenes may be the right choices[95, 96], because electrochemical active I terminal groups significantly promote the capacity of corresponding devices[97, 98]. Further, controllable synthesis macroporous MXene aerogels with high pore volume without sacrifice of conductivity are highly needed for high-mass-loading active materials, in this regard, template methods with controllable sizes and shapes of templates are feasible to construct ideal MXene-based hosts for high-performance cathodes[99–101]. MXene nanosheets based coating layers show great potentials for durable and dendrite-free Zn anodes. In contrast to MXene-based hosts for Zn, MXene nanosheets could be easily coated on commercial Zn foil anodes by available industrial technologies, such as spray coating, blade coating, and even printing technology, in which the small amount of MXene usage can significantly enhance the electrochemical performance of Zn anodes without sacrifice of energy density. Notably, the key is to precisely control the pores and zinc ion diffusion pathways in the MXene-based coating layers for unform Zn^{2+} ion flux, therefore, small organic molecules may be intercalated into the MXene nanosheets to tune the pores and Zn^{2+} diffusion channels. Meanwhile, strong coating interfaces should be established to withstand the volume variation of Zn anodes during stripping and plating processes, in this regard, novel material chemistry and coating technologies are highly needed to construct MXene-based coating layers on Zn anodes for high-performance ZHCs.

(3) MXene-based new-concept ZHCs. ZHCs with intrinsic safety show promising applications in wearable devices, and MXenes with excellent conductivity and mechanical flexibility are ideal active materials to construct new-concept ZHCs for future wearable and smart devices[102]. Recent studies demonstrate the powerful spinning synthesis of fiber-shaped ZHCs[103], enlightening the new-shaped ZHCs. Furthermore, other new-concepts are highly needed for next-generation ZHCs, such as anti-freezing ZHCs and self-healing ZHCs.

Lastly, the construction of advanced ZHCs is a systematic engineering, in addition to the anodes and cathodes of ZHCs discussed in this review, the selection of the electrolyte of ZHCs, the rational selection of cathode/electrolyte couples with new zinc storage mechanisms may provide a new way to construct high-performance ZHCs. Therefore, continuous innovations are highly needed for future MXene-based ZHCs.

Acknowledgements

This work was financially supported by LiaoNing Revitalization Talents Program (XLYC2007129), the Natural Science Foundation of Liaoning Province (2020-MS-095), the Fundamental Research Funds for the Central Universities of China (N2105008), and the CAS Key Laboratory of Carbon Materials (KLCMKFJJ2004).

References

[1] Chen H, Zheng Y, Zhu X Q, et al. Bamboo-derived porous carbons for Zn-ion hybrid supercapacitors[J]. Materials Research Bulletin, 2021, 139: 111281.

[2] Han L, Huang H L, Li J F, et al. A novel redox bromide-ion additive hydrogel electrolyte for flexible Zn-ion hybrid supercapacitors with boosted energy density and controllable zinc deposition[J]. Journal of Materials Chemistry A, 2020, 8(30): 15042-15050.

[3] Tang H, Yao J, Zhu Y. Recent developments and future prospects for zinc-ion hybrid capacitors: A review[J]. Advanced Energy Materials, 2021, 11(14): 2003994.

[4] Lu W, Yang Y, Zhang T, et al. Synergistic effects of Fe and Mn dual-doping in Co_3S_4 ultrathin nanosheets for high-performance hybrid supercapacitors[J]. Journal of Colloid and Interface Science, 2021, 590: 226-237.

[5] Yuan Z, Wang H, Shen J, et al. Hierarchical Cu_2S@NiCo-LDH double-shelled nanotube arrays with enhanced electrochemical performance for hybrid supercapacitors[J]. Journal of Materials Chemistry A, 2020, 8(42): 22163-22174.

[6] Zhang Z K, Zhang H X, Hou Y, et al. One-step synthesis of $CeFeO_3$ nanoparticles on porous-rich nanocarbon frameworks derived from ZIF-8 for boosted oxygen reduction reaction in pH value universal electrolytes[J]. J Mater Chem A, 2022.

[7] Panja T, Ajuria J, Díez N, et al. Fabrication of high-performance dual carbon Li-ion hybrid capacitor: Mass balancing approach to improve the energy-power density and cycle life[J]. Scientific Reports, 2020, 10(1): 1-11.

[8] Kim Y, Woo S C, Lee C S, et al. Electrochemical investigation on high-rate properties of graphene nanoplatelet-carbon nanotube hybrids for Li-ion capacitors[J]. Journal of Electroanalytical Chemistry, 2020, 863: 114060.

[9] Luo S N, Yuan T, Soule L K, et al. Enhanced ionic/electronic transport in nano-TiO_2/sheared CNT composite electrode for Na^+ insertion-based hybrid ion-capacitors[J]. Advanced Functional Materials, 2020, 30(5): 1908309.

[10] Huang F, Liu W, Wang Q, et al. Natural N/O-doped hard carbon for high performance K-ion hybrid capacitors[J]. Electrochimica Acta, 2020, 354: 136701.

[11] Li Y, Lu P, Shang P, et al. Pyridinic nitrogen enriched porous carbon derived from bimetal organic frameworks for high capacity zinc-ion hybrid capacitors with remarkable rate capability[J]. Journal of Energy Chemistry, 2021, 56: 404-411.

[12] Cui M, Xiao Y, Kang L, et al. Quasi-isolated Au particles as heterogeneous seeds to guide uniform Zn deposition for aqueous zinc-ion batteries[J]. ACS Applied Energy Materials, 2019, 2(9): 6490-6496.

[13] Li H, Yang Q, Mo F, et al. MoS_2 nanosheets with expanded interlayer spacing for rechargeable aqueous Zn-ion batteries[J]. Energy Storage Materials, 2019, 19: 94-101.

[14] Mo F, Chen Z, Liang G, et al. Zwitterionic sulfobetaine hydrogel electrolyte building separated positive/negative ion migration channels for aqueous Zn-MnO_2 batteries with superior rate capabilities[J]. Advanced Energy Materials, 2020, 10(16): 2000035.

[15] Qian L, Yao W, Yao R, et al. Cations coordination-regulated reversibility enhancement for aqueous Zn-ion battery[J]. Advanced Functional Materials, 2021, 31(40): 2105736.

[16] Zhu C Y, Ye Y W, Guo X, et al. Design and synthesis of carbon-based nanomaterials for electrochemical energy storage[J]. New Carbon Materials, 2022, 37(1): 59-92.

[17] Wang M, Che X G, Liu S Y, et al. A review of carbon-based cathode materials for zinc-ion capacitors[J]. New Carbon Materials, 2021, 36(1): 155-166.

[18] Shang P, Liu M, Mei Y, et al. Urea-mediated monoliths made of nitrogen-enriched mesoporous carbon nanosheets for high-performance aqueous zinc ion hybrid capacitors[J]. Small, 2022, 18: 2108057.

[19] Wang S, Wang Q, Zeng W, et al. A new free-standing aqueous zinc-ion capacitor based on MnO_2-CNTs cathode and MXene anode[J]. Nano-Micro Letters, 2019, 11(1): 1-12.

[20] Chaudhari N K, Jin H, Kim B, et al. MXene: An emerging two-dimensional material for future energy conversion and storage applications[J]. Journal of Materials Chemistry A, 2017, 5(47): 24564-24579.

[21] Alhabeb M, Maleski K, Anasori B, et al. Guidelines for synthesis and processing of two-dimensional titanium carbide ($Ti_3C_2T_x$ MXene)[J]. Chemistry of Materials, 2017, 29(18): 7633-7644.

[22] Sang X, Xie Y, Lin M W, et al. Atomic defects in monolayer titanium carbide ($Ti_3C_2T_x$) MXene[J]. ACS Nano, 2016, 10(10): 9193-9200.

[23] Dillon A D, Ghidiu M J, Krick A L, et al. Highly conductive optical quality solution-processed films of 2D titanium carbide[J]. Advanced Functional Materials, 2016, 26(23): 4162-4168.

[24] Lipatov A, Lu H, Alhabeb M, et al. Elastic properties of 2D $Ti_3C_2T_x$ MXene monolayers and bilayers[J]. Science Advances, 2018, 4(6): eaat0491.

[25] Kong F, He X, Liu Q, et al. Effect of Ti_3AlC_2 precursor on the electrochemical properties of the resulting MXene Ti_3C_2 for Li-ion batteries[J]. Ceramics International, 2018, 44(10): 11591-11596.

[26] Maleski K, Mochalin V N, Gogotsi Y. Dispersions of two-dimensional titanium carbide MXene in organic solvents[J]. Chemistry of Materials, 2017, 29(4): 1632-1640.

[27] Firouzjaei M D, Karimiziarani M, Moradkhani H, et al. MXenes: The two-dimensional influencers[J]. Materials Today Advances, 2022, 13: 100202.

[28] Okubo M, Sugahara A, Kajiyama S, et al. MXene as a charge storage host[J]. Accounts of Chemical Research, 2018, 51(3): 591-599.

[29] Sun S, Liao C, Hafez A M, et al. Two-dimensional MXenes for energy storage[J]. Chemical Engineering Journal, 2018, 338: 27-45.

[30] Kumar P, Singh S, Hashmi S A R, et al. MXenes: Emerging 2D

materials for hydrogen storage[J]. Nano Energy, 2021, 85: 105989.

[31] Shinde P A, Patil A M, Lee S, et al. Two-dimensional MXenes for electrochemical energy storage applications[J]. Journal of Materials Chemistry A, 2022, 10: 1105-1149.

[32] Wang Q, Wang S, Guo X, et al. Mxene-reduced graphene oxide aerogel for aqueous zinc-ion hybrid supercapacitor with ultralong cycle life[J]. Advanced Electronic Materials, 2019, 5(12): 1900537.

[33] Li X, Li M, Yang Q, et al. Vertically aligned Sn^{4+} preintercalated Ti_2CT_x MXene sphere with enhanced Zn-ion transportation and superior cycle lifespan[J]. Advanced Energy Materials, 2020, 10(35): 2001394.

[34] Cui H, Mi H, Ji C, et al. A durable MXene-based zinc-ion hybrid supercapacitor with sulfated polysaccharide reinforced hydrogel/electrolyte[J]. Journal of Materials Chemistry A, 2021, 9(42): 23941-23954.

[35] Chen J, Chen H, Chen M, et al. Nacre-inspired surface-engineered MXene/nanocellulose composite film for high-performance supercapacitors and zinc-ion capacitors[J]. Chemical Engineering Journal, 2022, 428: 131380.

[36] Yang Q, Huang Z, Li X, et al. A wholly degradable, rechargeable Zn-Ti_3C_2 MXene capacitor with superior anti-self-discharge function[J]. ACS Nano, 2019, 13(7): 8275-8283.

[37] Tian Y, An Y, Wei C, et al. Flexible and free-standing $Ti_3C_2T_x$ MXene@Zn paper for dendrite-free aqueous zinc metal batteries and nonaqueous lithium metal batteries[J]. ACS Nano, 2019, 13(10): 11676-11685.

[38] An Y, Tian Y, Liu C, et al. Rational design of sulfur-doped three-dimensional $Ti_3C_2T_x$ MXene/ZnS heterostructure as multifunctional protective layer for dendrite-free zinc-ion batteries[J]. ACS Nano, 2021, 15(9): 15259-15273.

[39] Li X, Li Q, Hou Y, et al. Toward a practical Zn powder anode: $Ti_3C_2T_x$ MXene as a lattice-match electrons/ions redistributor[J]. ACS Nano, 2021, 15(9): 14631-14642.

[40] Wang H, Ye W, Yang Y, et al. Zn-ion hybrid supercapacitors: Achievements, challenges and future perspectives[J]. Nano Energy, 2021, 85: 105942.

[41] Yin J, Zhang W, Alhebshi N A, et al. Electrochemical zinc-ion capacitors: Fundamentals, materials, and systems[J]. Advanced Energy Materials, 2021, 11(21): 2100201.

[42] Naguib M, Kurtoglu M, Presser V, et al. Two-dimensional nanocrystals produced by exfoliation of Ti_3AlC_2[J]. Advanced Materials, 2011, 23(37): 4248-4253.

[43] Augustyn V, Simon P, Dunn B. Pseudocapacitive oxide materials for high-rate electrochemical energy storage[J]. Energy Environmental Science, 2014, 7(5): 1597-1614.

[44] Jagadale A D, Rohit R C, Shinde S K, et al. Materials development in hybrid zinc-ion capacitors[J]. ChemNanoMat, 2021, 7(10): 1082-1098.

[45] Wang L, Peng M, Chen J, et al. High energy and power zinc-ion capacitors: A dual-ion adsorption and reversible chemical adsorption coupling mechanism[J]. ACS Nano, 2022, 16(2): 2877-2888.

[46] Zhang H, Liu Q, Fang Y, et al. Boosting Zn-ion energy storage capability of hierarchically porous carbon by promoting chemical adsorption[J]. Advanced Materials, 2019, 31(44): 1904948.

[47] Zheng Y, Zhao W, Jia D, et al. Porous carbon prepared via combustion and acid treatment as flexible zinc-ion capacitor electrode material[J]. Chemical Engineering Journal, 2020, 387: 124161.

[48] Liu P, Liu W, Huang Y, et al. Mesoporous hollow carbon spheres boosted, integrated high performance aqueous Zn-ion energy storage[J]. Energy Storage Materials, 2020, 25: 858-865.

[49] Deng X, Li J, Shan Z, et al. A N, O co-doped hierarchical carbon cathode for high-performance Zn-ion hybrid supercapacitors with enhanced pseudocapacitance[J]. Journal of Materials Chemistry A, 2020, 8(23): 11617-11625.

[50] Yin J, Zhang W, Wang W, et al. Electrochemical zinc-ion capacitors enhanced by redox reactions of porous carbon cathodes[J]. Advanced Energy Materials, 2020, 10(37): 2001705.

[51] Zhang W, Jiang H, Li Y, et al. Pizza-like heterostructured $Ti_3C_2T_x/Bi_2S_3$@NC with ultra-high specific capacitance as a potential electrode material for aqueous zinc-ion hybrid supercapacitors[J]. Journal of Alloys and Compounds, 2021, 883: 160881.

[52] Mathis T S, Kurra N, Wang X, et al. Energy storage data reporting in perspective-guidelines for interpreting the performance of electrochemical energy storage systems[J]. Advanced Energy Materials, 2019, 9(39): 1902007.

[53] Balducci A, Belanger D, Brousse T, et al. Perspective-a guideline for reporting performance metrics with electrochemical capacitors: From electrode materials to full devices[J]. Journal of The Electrochemical Society, 2017, 164(7): A1487.

[54] Wang C, Zeng X, Cullen P J, et al. The rise of flexible zinc-ion hybrid capacitors: Advances, challenges, and outlooks[J]. Journal of Materials Chemistry A, 2021, 9: 19054-19082.

[55] Brousse T, Bélanger D, Long J W. To be or not to be pseudocapacitive?[J]. Journal of The Electrochemical Society, 2015, 162(5): A5185.

[56] Shao Y, Sun Z, Tian Z, et al. Regulating oxygen substituents with optimized redox activity in chemically reduced graphene oxide for aqueous Zn-ion hybrid capacitor[J]. Advanced Functional Materials, 2021, 31(6): 2007843.

[57] Chen Z, Li X, Wang D, et al. Grafted MXene/polymer electrolyte for high performance solid zinc batteries with enhanced shelf life at low/high temperatures[J]. Energy & Environmental Science, 2021, 14(6): 3492-3501.

[58] Li X, Li N, Huang Z, et al. Confining aqueous Zn-Br halide redox chemistry by $Ti_3C_2T_x$ MXene[J]. ACS Nano, 2021, 15(1): 1718-1726.

[59] Liu F, Jin S, Xia Q, et al. Research progress on construction and energy storage performance of MXene heterostructures[J].

Journal of Energy Chemistry, 2021, 62: 220-242.

[60] Etman A S, Halim J, Rosen J. $Mo_{1.33}CT_z$-$Ti_3C_2T_z$ mixed MXene freestanding films for zinc-ion hybrid supercapacitors[J]. Materials Today Energy, 2021, 22: 100878.

[61] Li F, Liu Y, Wang G G, et al. 3D porous H-$Ti_3C_2T_x$ films as free-standing electrodes for zinc ion hybrid capacitors[J]. Chemical Engineering Journal, 2022, 435: 135052.

[62] Fan Z, Jin J, Li C, et al. 3D-printed Zn-ion hybrid capacitor enabled by universal divalent cation-gelated additive-free Ti_3C_2 MXene ink[J]. ACS Nano, 2021, 15(2): 3098-3107.

[63] Shi B, Li L, Chen A, et al. Continuous fabrication of $Ti_3C_2T_x$ MXene-Based braided coaxial zinc-ion hybrid supercapacitors with improved performance[J]. Nano-Micro Letters, 2022, 14(1): 1-10.

[64] Peng M, Wang L, Li L, et al. Manipulating the interlayer spacing of 3D MXenes with improved stability and zinc-ion storage capability[J]. Advanced Functional Materials, 2022, 32: 2109524.

[65] Maughan P A, Tapia-Ruiz N, Bimbo N. In-situ pillared MXene as a viable zinc-ion hybrid capacitor[J]. Electrochimica Acta, 2020, 341: 136061.

[66] Jin Y, Ao H, Qi K, et al. A high-rate, long life, and anti-self-discharge aqueous N-doped Ti_3C_2/Zn hybrid capacitor[J]. Materials Today Energy, 2021, 19: 100598.

[67] Li Y, Zhang W, Yang X, et al. A high-voltage and high-capacity $Ti_3C_2T_x$/$BiCuS_{2.5}$ heterostructure to boost up the energy density and recyclability of zinc-ion hybrid capacitors[J]. Nano Energy, 2021, 87: 106136.

[68] Wang C, Wei S, Chen S, et al. Delaminating vanadium carbides for zinc-ion storage: Hydrate precipitation and H^+/Zn^{2+} co-action mechanism[J]. Small Methods, 2019, 3(12): 1900495.

[69] Cao Z, Fu J, Wu M, et al. Synchronously manipulating Zn^{2+} transfer and hydrogen/oxygen evolution kinetics in MXene host electrodes toward symmetric Zn-ions micro-supercapacitor with enhanced areal energy density[J]. Energy Storage Materials, 2021, 40: 10-21.

[70] Cheng W, Fu J, Hu H, et al. Interlayer structure engineering of MXene-based capacitor-type electrode for hybrid micro-supercapacitor toward battery-level energy density[J]. Advanced Science, 2021, 8(16): 2100775.

[71] Liu P, Liu W, Liu K. Rational modulation of emerging MXene materials for zinc-ion storage[J]. Carbon Energy, 2021, 4(1): 60-76.

[72] Li F, Liu Y L, Wang G G, et al. The design of flower-like C-MnO_2 nanosheets on carbon cloth toward high-performance flexible zinc-ion batteries[J]. Journal of Materials Chemistry A, 2021, 9(15): 9675-9684.

[73] Zhang Y, Deng S, Pan G, et al. Introducing oxygen defects into phosphate ions intercalated manganese dioxide/vertical multilayer graphene arrays to boost flexible zinc ion storage[J]. Small Methods, 2020, 4(6): 1900828.

[74] Zhang Y Z, Wang Y, Jiang Q, et al. MXene printing and patterned coating for device applications[J]. Advanced Materials, 2020, 32(21): 1908486.

[75] Fu K K, Cheng J, Li T, et al. Flexible batteries: From mechanics to devices[J]. ACS Energy Letters, 2016, 1(5): 1065-1079.

[76] Wang J, Wang J G, Liu H, et al. A highly flexible and lightweight MnO_2/graphene membrane for superior zinc-ion batteries[J]. Advanced Functional Materials, 2021, 31(7): 2007397.

[77] Li X, Ma X, Hou Y, et al. Intrinsic voltage plateau of a Nb_2CT_x MXene cathode in an aqueous electrolyte induced by high-voltage scanning[J]. Joule, 2021, 5(11): 2993-3005.

[78] Ding B, Ong W J, Jiang J, et al. Uncovering the electrochemical mechanisms for hydrogen evolution reaction of heteroatom doped M_2C MXene (M=Ti, Mo)[J]. Applied Surface Science, 2020, 500: 143987.

[79] Liu H, Wang J G, Hua W, et al. Building Ohmic contact interfaces toward ultrastable Zn metal anodes[J]. Advanced Science, 2021, 8(23): 2102612.

[80] Liu H, Wang J G, You Z, et al. Rechargeable aqueous zinc-ion batteries: Mechanism, design strategies and future perspectives[J]. Materials Today, 2021, 42: 73-98.

[81] Li Z, Guo D, Wang D, et al. Exploration of metal/Ti_3C_2 MXene-derived composites as anode for high-performance zinc-ion supercapacitor[J]. Journal of Power Sources, 2021, 506: 230197.

[82] Li X, Li M, Luo K, et al. Lattice matching and halogen regulation for synergistically induced uniform zinc electrodeposition by halogenated Ti_3C_2 MXenes[J]. ACS Nano, 2022, 16: 813-822.

[83] Zhou J, Xie M, Wu F, et al. Encapsulation of metallic Zn in a hybrid MXene/graphene aerogel as a stable Zn anode for foldable Zn-ion batteries[J]. Advanced Materials, 2022, 34: 2106897.

[84] Zhang Y, Cao Z, Liu S, et al. Charge - enriched strategy based on MXene-based polypyrrole layers toward dendrite-free Zinc metal anodes[J]. Advanced Energy Materials, 2022, 12: 2103979.

[85] Xue Y, Zhang Q, Wang W, et al. Opening two-dimensional materials for energy conversion and storage: A concept[J]. Advanced Energy Materials, 2017, 7(19): 1602684.

[86] Wu Z, Shang T, Deng Y, et al. The assembly of MXenes from 2D to 3D[J]. Advanced Science, 2020, 7(7): 1903077.

[87] Li K, Liang M, Wang H, et al. 3D MXene architectures for efficient energy storage and conversion[J]. Advanced Functional Materials, 2020, 30(47): 2000842.

[88] Liu Y H, Wang C Y, Yang S L, et al. 3D MXene architectures as sulfur hosts for high-performance lithium-sulfur batteries[J]. Journal of Energy Chemistry, 2022, 66: 429-439.

[89] Shan Y H, Li L B, Du J T, et al. High performance lithium-sulfur batteries using three-dimensional hierarchical porous carbons to host the sulfur[J]. New Carbon Materials, 2021, 36(6): 1094-1102.

[90] Xiong D, Shi Y, Yang H Y. Rational design of MXene-based films for energy storage: Progress, prospects[J]. Materials Today, 2021, 46: 183-211.

[91] Wei C, Tao Y, An Y, et al. Recent advances of emerging 2D MXene for stable and dendrite-free metal anodes[J]. Advanced Functional Materials, 2020, 30(45): 2004613.

[92] Zhan X, Si C, Zhou J, et al. MXene and MXene-based composites: Synthesis, properties and environment-related applications[J]. Nanoscale Horizons, 2020, 5(2): 235-258.

[93] Zhan C, Naguib M, Lukatskaya M, et al. Understanding the MXene pseudocapacitance[J]. The Journal of Physical Chemistry Letters, 2018, 9(6): 1223-1228.

[94] Wang X, Wang Z, Qiu J. Stabilizing MXene by hydration chemistry in aqueous solution[J]. Angewandte Chemie International Edition, 2021, 60(51): 26587-26591.

[95] Li M, Li X, Qin G, et al. Halogenated Ti_3C_2 MXenes with electrochemically active terminals for high-performance zinc ion batteries[J]. ACS Nano, 2021, 15(1): 1077-1085.

[96] Li Y, Shao H, Lin Z, et al. A general Lewis acidic etching route for preparing MXenes with enhanced electrochemical performance in non-aqueous electrolyte[J]. Nature Materials, 2020, 19(8): 894-899.

[97] Ren Z, Yu J, Li Y, et al. Tunable free-standing ultrathin porous nickel film for high performance flexible nickel-metal hydride batteries[J]. Advanced Energy Materials, 2018, 8(12): 1702467.

[98] Li H, Ma L, Han C, et al. Advanced rechargeable zinc-based batteries: Recent progress and future perspectives[J]. Nano Energy, 2019, 62: 550-587.

[99] Huang H, Jiang R, Feng Y, et al. Recent development and prospects of surface modification and biomedical applications of MXenes[J]. Nanoscale, 2020, 12(3): 1325-1338.

[100] Riazi H, Anayee M, Hantanasirisakul K, et al. Surface modification of a MXene by an aminosilane coupling agent[J]. Advanced Materials Interfaces, 2020, 7(6): 1902008.

[101] Wang D, Li F, Lian R, et al. A general atomic surface modification strategy for improving anchoring and electrocatalysis behavior of $Ti_3C_2T_2$ MXene in lithium-sulfur batteries[J]. ACS Nano, 2019, 13(10): 11078-11086.

[102] Chao H, Qin H, Zhang M, et al. Boosting the pseudocapacitive and high mass-loaded lithium/sodium storage through bonding polyoxometalate nanoparticles on MXene nanosheets[J]. Advanced Functional Materials, 2021, 31(16): 2007636.

[103] Chen Q, Cao L, Wang H, et al. Oxygen/fluorine-functionalized flexible carbon electrodes for high-performance and anti-self-discharge Zn-ion hybrid capacitors[J]. Journal of Power Sources, 2022, 538: 231586.